

Solid-State Polymerization of Poly(ethylene terephthalate). II. Modeling Study of the Reaction Kinetics and Properties

T. Y. Kim, S. A. Jabarin

Polymer Institute and Department of Chemical and Environmental Engineering, University of Toledo, Toledo, Ohio 43606-3390

Received 7 March 2002; accepted 10 August 2002

ABSTRACT: Comprehensive modeling studies were used to describe the kinetics of the solid-state polymerization (SSP) of poly(ethylene terephthalate). The validity of the model was confirmed by the successful fitting of the experimental results for molecular weight increases, at temperatures ranging from 180 to 230°C and for times up to 12 h, with one fitting parameter. The changes in the concentrations for hydroxyl end groups ([—OH]), carboxyl end groups ([—COOH]), vinyl end groups, and terephthalic acid (TPA) were simulated with the model. During SSP, the contents of not only hydroxyl and carboxyl end groups but also vinyl ester end groups and TPA monomer were pre-

dicted to decrease as a function of the SSP time and temperature. The effects of the pellet size and the molar ratio of carboxyl end groups to hydroxyl end groups were also calculated. At an end-group molar ratio ([—COOH]/[—OH]) of around 0.7, a maximum SSP rate was obtained. As the [—COOH]/[—OH] ratio increased, the contents of the vinyl end groups and TPA monomer were predicted to increase. © 2003 Wiley Periodicals, Inc. *J Appl Polym Sci* 89: 213–227, 2003

Key words: solid-state polymerization; modeling; polyesters

INTRODUCTION

Solid-state polymerization (SSP) has been used as an efficient way to increase the molecular weight of a polymer. In the first article of this series,¹ an experimental study was performed to investigate the effects of the precursor intrinsic viscosity (IV) on the SSP kinetics and properties. Several conclusions resulted from these investigations. SSP was observed to proceed under more than one kinetic mechanism. For reaction temperatures ranging from 200 to 230°C, it was proposed that the end-group diffusion step, representing chain mobility, and the byproduct diffusion step were rate-determining steps. In addition, the ratio of end groups ([—COOH]/[—OH]) was observed to play an important role in the kinetics of SSP. Although experimental studies are an efficient means for comparing kinetic and material properties, the information that can be obtained is limited in terms of the mechanisms, side reactions, and concentrations of various components involved in SSP. In this work, a comprehensive modeling study was performed with a modification of Kang's model. Various SSP mechanisms were considered in detail, and additional information was obtained about many side reactions, their product concentrations, the effects of the pellet size,

and the effects of the initial molar ratio of the end groups. Before we introduce the model, we present a brief review of published SSP kinetic modeling techniques.

Kinetic studies of SSP

The overall reaction rate of SSP depends on both chemical and physical processes. Several processes can be considered for analyzing the kinetics of SSP. Many researchers^{2–9} have reported three steps: (1) reversible chemical reactions between molecular chain end groups, (2) diffusion of the volatile byproducts [ethylene glycol (EG), water (W), and acetaldehyde (AA)] in the solid polymer, and (3) diffusion of the volatile byproducts from the polymer surface to the inert gas. The third process, the diffusion into the gas phase, has often been ignored because its rate is high in comparison with the others. Some recently published reports^{10,11} discuss another process, the diffusion of end groups before a reaction in the solid phase. Researchers consider this an important process for several reasons. There exist intrinsic differences between polymerization reactions in the solid phase and those in the melt phase. There are many factors causing these differences. For example, molecular chain mobility is believed to decrease more drastically as temperatures decrease below a polymer's melting point, which strongly affects the reaction rates. In addition, activation energies much higher than the activation energies generally reported for reactions in the melt phase must be required to explain the large

Correspondence to: S. A. Jabarin (sjabari@utnet.utoledo.edu).

Contract grant sponsor: PET Industrial Consortium.

decreases in the reaction rate constants. Crystallization occurs during SSP and is another factor that complicates an estimation of reaction rate constants, which also affect chain mobility. Several techniques have been published to consider the process of end-group diffusion. These are described later in more detail when the four steps are considered for an analysis of the kinetics of SSP.

Many approaches have been used to investigate SSP kinetics. One means of investigation is the experimental approach. Some researchers^{12,13} have tried to make empirical SSP models by fitting the molecular weight against the square root of the reaction time, implying that the diffusion process is involved in the SSP process. This approach gives apparent rate constants involving all the mechanisms taking place and is convenient for comparing SSP rates. It has limitations, however, in that little information can be obtained about individual mechanisms. Experimental approaches can, nevertheless, be successfully used as a way to discern the rate-determining mechanisms. Huang and Walsh⁴ tried to find important mechanisms in SSP kinetics by investigating the effect of numerous variables on the SSP rate. From the importance of each variable, the mechanism that is acting as the rate-determining step can be identified at a certain condition of SSP. Chen and Chen¹⁰ also reported an empirical model. Even though that model appears to have been made intuitively rather than by a theoretical approach, it was the first to deal with the end-group diffusion mechanism.

Depending on the process and operating variables, the overall SSP rate can be controlled by one or more of these steps.⁴⁻⁶ Once important mechanisms have been identified, a model can be made and used to predict the kinetics of SSP. A modeling approach, based on SSP mechanisms, is the second means of investigating SSP kinetics. These models are different from the purely empirical ones previously described because they are based on assumptions regarding one or more controlling mechanisms. In the early times of SSP modeling studies, most models^{5,7,8,14} dealt with the main polymerization reactions to describe SSP kinetics. The majority of these models considered only ester-interchange reactions, but some models also included esterification reactions. Later, researchers^{9,11,15-17} began to consider many chemical reactions, including esterification reactions and even various side reactions. They denoted their advanced models as comprehensive models in contrast to the previous simple models dealing only with ester-interchange reactions. There are some differences in the mathematical techniques used in the models. Analytical methods were often tried in the initial simple models, whereas numerical approaches have generally been used in the comprehensive models because of the many equations and variables in the models. The more recent models also differ in the number of rate-con-

trolling steps being assumed. In the initial simple models, only one assumption (the ester-interchange reaction control or EG diffusion control) was generally made about SSP mechanisms so that the system could be simplified to obtain an analytical solution. The recent comprehensive models do not require much simplification to solve the system so that they can be made based on more than one rate-controlling assumption with help from numerical techniques and computers. Many mechanisms in SSP kinetics, such as chemical reactions and the diffusion of byproducts, can be considered together in the comprehensive models.

Table I gives a brief summary and classification of published SSP models. It is not always straightforward to classify published SSP models by specified criteria. Despite these difficulties, a classification of SSP models is given to clarify the various modeling ideas and their progress regarding SSP kinetics. According to the mechanisms being assumed, models can be divided into several categories. First, there are reaction models that assume that the chemical reaction is the rate-controlling step. This assumption has been known to hold at the conditions of very low reaction temperatures and very small particle sizes.^{2,3,5,6,14} Under these conditions, the diffusion is fast in comparison with the chemical reaction and can be ignored. In these cases, the concentrations of byproducts can be assumed to be zero, the reactions become irreversible, and the molecular weight increases linearly with respect to the reaction time. As the temperature increases above 200°C, however, these models usually fail to follow observed SSP kinetic characteristics that exhibit nonlinear behavior for molecular weight increases with time.

Second, the diffusion model can be considered. Many researchers⁵⁻⁹ have tried to analyze SSP kinetics with this kind of model because it can fit the behavior of molecular weight increases successfully. When models assume diffusion control (simple diffusion models), the chemical reaction is assumed to be so fast to reach equilibrium that it can be ignored. The concentrations of EG can be converted into hydroxyl end-group concentrations with equilibrium assumptions, and this provides the molecular weight of the polymer.^{5,6}

When comprehensive models considered chemical reactions together with diffusion,^{9,17} the same kinetic parameters, such as frequency factors, activation energies, and equilibrium constants for chemical reactions, were used that were used for melt-phase polymerization. The diffusivities of byproducts, difficult to measure experimentally, were generally used as fitting parameters for the experimental data. Most researchers using this approach^{6,8,9,17} reported activation energies of about 30 kcal/mol from the temperature dependency of the diffusivity values. This value of 30 kcal/mol for the activation energy, however,

TABLE I
Classification of SSP Models Published

	Reaction model	Diffusion model	Comprehensive model	Modified comprehensive model
Number of reactions	Simple models, consider only main reactions		Comprehensive models, consider many reactions, including side reactions	
Rate-determining step	Chemical reaction	Byproduct diffusion	Chemical reaction, byproduct diffusion	End-group diffusion (chain mobility), chemical reaction, byproduct diffusion
Estimation of reaction rate	Data fit (to estimate rate constant)	Assuming a fast reaction and equilibrium	Using melt phase data for rate constants (E_a , A)	Data fit Adjusts reaction rates by considering one of the following Modified rate constants (k 's) due to chain mobility limitation Effective concentrations (c 's) due to end-group diffusion
Byproduct diffusivity	Not required (fast diffusion)	From data fit ($E_a \sim 30$ kcal/mol)		From free volume theory ($E_a \sim 4-5$ kcal/mol)
Features	Linear IV growth Irreversible reaction Works only at low temperatures	Considers Byproduct diffusion Reversible reaction Nonlinear growth of IV E_a too high for diffusion		Considers an adjusted reaction rate in the solid phase, limited end-group mobility Byproduct diffusion Reversible chemical reactions Nonlinear growth of IV
Important variables	Temperature, time, reaction rate constants	Temperature, time, diffusivity (crystallinity), equilibrium constants, pellet size		Temperature, time, pellet size, diffusivity (crystallinity), rate constants (or effective end-group concentration)
References	2, 3, 5, 12-14, 18 ^a	5, 6, 8	9, 17	11, 15, 16

E_a , activation energy; A , frequency factor.

^a The authors of ref. 18 showed a nonlinear increase in molecular weight by introduction of the concept of inactive end groups.

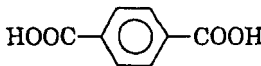
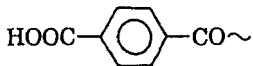
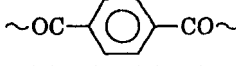
caused some disagreement among researchers^{5,15} because the activation energies for diffusion cannot be greater than those of the chemical reactions (known to be ca. 20 kcal/mol). The chemical reaction step becomes the rate-determining step with decreasing temperature. Therefore, the chemical reaction step must have a higher temperature sensitivity and a higher activation energy than the diffusion step.⁵

As a next stage in the history of SSP modeling, researchers began to consider the concept of end-group diffusion.^{10,11,15,16} Duh¹⁸ performed SSP experiments with finely powdered poly(ethylene terephthalate) (PET), in which byproduct diffusion limitations could be ignored, and showed that molecular weights still increased nonlinearly at temperatures ranging from 200 to 230°C. The reaction-controlling model fails to work at high temperatures above 200°C, even under conditions of very small particle sizes. This is because the molecular weight increases in a nonlinear way at high temperatures, even in the case of very fine powders.¹⁸ Additional evidence for end-group diffusion limitations can be inferred from the argument regarding activation energies in the diffusion models. As

described earlier, most diffusion models^{6,8,9} report activation energy values that are too high (near 30 kcal/mol) with diffusivities as fitting parameters and with melt-phase kinetic parameters applied for chemical reaction rates. This means that actual SSP rates decrease much more as temperatures decrease than expected by extrapolation from melt-phase kinetic data. All these results suggest strongly that the diffusion of byproducts and the chemical reactions that were identified in the melt phase are not the only rate-determining steps and that there must be another factor controlling SSP rates. The diffusion of chain end groups was suggested as an additional rate-determining mechanism.

Several ways to consider this end-group diffusion have been published. Wu et al.¹¹ assumed the steady state for the diffusion of chain end groups and chemical reactions. Effective concentrations of end groups were considered, which are different from the bulk concentrations because of the diffusion limitations of chain end groups applied to a local space in PET pellets. Duh¹⁸ introduced the concept of inactive end groups in his pure reaction model. Inactive end

TABLE II
Ten Components Considered in Kang's Model¹⁵

Abbreviation	Description	Molecular structure
TPA	Terephthalic acid	
EG	Ethylene glycol	HOCH ₂ CH ₂ OH
W	Water	H ₂ O
tEG	EG end group	HOCH ₂ CH ₂ O~
tTPA	TPA end group	
bEG	EG repeat unit	~OCH ₂ CH ₂ O~
bTPA	TPA repeat unit	
bDEG	Diethylene glycol repeat unit	~OCH ₂ CH ₂ OCH ₂ CH ₂ O~
tVIN	Vinyl end group	CH ₂ =CHO~
AA	Acetaldehyde	CH ₃ CHO

groups were defined as the end groups that could not participate in the reactions for many reasons, the isolation of end groups between crystalline structures being one of them. Even though he did not mention end-group diffusion in his article, through the introduction of the concept of inactive end groups, essentially similar effects of decreases in SSP rates could be obtained as when end-group diffusion had been considered. Other researchers, such as Kang¹⁵ and Devotta and Mashelkar,¹⁶ assumed that the kinetic rate constants for the intermolecular reactions were affected by the mobility of molecular chain ends. They proposed appropriate expressions for the chain mobility and included these terms in the kinetic rate constants for the intermolecular reactions. In these approaches, the diffusivities for the reaction byproducts were generally estimated with the free volume theory, which assumes that diffusivities can be expressed as functions of the size and shape of diffusing molecules, the volume fraction of the amorphous phase, and the reaction temperature.

Some properties affected by SSP

The changes in the properties of PET during SSP, especially in relation to the crystalline phase, were discussed previously.¹ The crystallinity, crystallite size, and melting points are included among these properties. This modeling study can be related to other properties of PET. The main purpose of SSP is to increase the molecular weight of the polymeric material. SSP also influences some additional properties of PET that are considered important for food packaging applications. AA in containers and films is important because it can affect the flavor of contents.¹⁹ For the AA concentration to be kept low in container or film materials, PET resins must have low initial contents of AA and good thermal stability so that minimal AA will be generated during the molding process. Many factors can be related to the resin's thermal stability in

terms of AA generation. The content of the vinyl ester (VIN) end group is one of the factors because it is known as an intermediate material in the degradation reaction path producing AA.^{19,20} It is important to identify how these components (AA and vinyl ester end groups) change during SSP and how their concentrations depend on SSP conditions.

The sublimation of terephthalic acid (TPA) can cause an additional problem in the PET molding process. Because TPA sublimates near 300°C,^{20,21} white powder, mostly TPA, can easily form from PET during the processes and affect processability and, sometimes, the quality of the molded products. It is, therefore, important to monitor variations in the TPA monomer content as a function of SSP conditions.

Even though many modeling studies have been performed on the SSP of PET, most researchers have focused on the kinetics and the changes in the molecular weight without mentioning the changes in the properties with respect to the aforementioned information. The purpose of this study was to apply a comprehensive SSP model to the results of experimental studies and to obtain information with significance in terms of PET properties, including the molecular weight, and concentrations of hydroxyl end groups, carboxyl end groups, vinyl ester end groups, residual AA, and TPA monomer.

SSP MODELING BASED ON KANG'S MODEL¹⁵

In this work, a model for the SSP of PET was applied, based on the one proposed by Kang.¹⁵ This model is a particle model that describes the SSP process in a single PET pellet. Therefore, the system is a single pellet in the SSP reactor. Mass transfer in the gas phase is neglected according to the assumption that the inert gas flow rate is high enough to avoid any limitation in the SSP rate. The model considers 10 components and 9 chemical reactions, as shown in Tables II and III.

TABLE III
Nine Chemical Reactions Considered in Kang's Model¹⁵

No.	Reactions	Rate constants (forward, reverse)
1	EG + TPA \rightleftharpoons tEG + tTPA + W	$k_1, k_1/K_1$
2	EG + tTPA \rightleftharpoons tEG + bTPA + W	$k_2, k_2/K_2$
3	tEG + TPA \rightleftharpoons bEG + tTPA + W	$k_3, k_3/K_3$
4	tEG + tTPA \rightleftharpoons bEG + bTPA + W	$k_4, k_4/K_4$
5	tEG + tEG \rightleftharpoons bEG + EG	$k_5, k_5/K_5$
6	tEG + tEG \rightarrow bDEG + W	$k_6, —$
7	bEG + bTPA \rightarrow tVIN + tTPA	$k_7, —$
8	tEG + bTPA \rightarrow AA + tTPA	$k_8, —$
9	tEG + tVIN \rightarrow bEG + AA	$k_9, —$

Components preceded by "t" are terminal end groups, while those preceded by "b" are backbone repeat units within the chain.

During SSP, the unsteady-state diffusion of the volatile byproducts is coupled with the chemical reactions. The mass balance equations of volatile components in a spherical PET particle can be written as follows:

$$\frac{\partial C_j}{\partial t} = D_j \left[\frac{\partial^2 C_j}{\partial r^2} + \frac{2}{r} \frac{\partial C_j}{\partial r} \right] + G_j(t) \quad (1)$$

where j is EG, W, or AA; C_j is the concentration of component j ; t is the reaction time; D_j is the diffusion coefficient of volatile component j ; and r is the distance from the center of the sphere (as long as the pellet has a spherical geometry). These three equations, obtained by the three components (EG, W, and AA) each being applied to eq. (1), were solved numerically with the Crank–Nicholson method.²²

The mass balance equations of nondiffusing components can be written as follows. In this case, the seven equations, obtained by each of the seven components (TPA, tEG, tTPA, bEG, bTPA, bDEG, and VIN) being applied to eq. (2), were solved numerically with the fourth-order Runge–Kutta method.²²

$$\frac{dC_j}{dt} = G_j(t) \quad (2)$$

where j is TPA, tEG, tTPA, bEG, bTPA, bDEG, or VIN. In eqs. (1) and (2), $G_j(t)$ is the generation rate due to

TABLE IV
 $G_j(t)$ of Each Component

$G_{EG}(t)$	$= -R_1 - R_2 + R_5$
$G_{TPA}(t)$	$= -R_1 - R_3$
$G_{tEG}(t)$	$= R_1 + R_2 - R_3 - R_4 - 2R_5 - 2R_6 - R_8 - R_9$
$G_{tTPA}(t)$	$= R_1 - R_2 + R_3 - R_4 + R_7 + R_8$
$G_{bEG}(t)$	$= R_3 + R_4 + R_5 - R_7 + R_9$
$G_{bTPA}(t)$	$= R_2 + R_4 - R_7 - R_9$
$G_W(t)$	$= R_1 + R_2 + R_3 + R_4 + R_6$
$G_{bDEG}(t)$	$= R_6$
$G_{tVIN}(t)$	$= R_7 - R_9$
$G_{AA}(t)$	$= R_8 + R_9$

TABLE V
Reaction Rate (R_i) of Each Reaction

$R_1 = \Phi_A R'_1 = \Phi_A \left[4k_1 \frac{C_{EG}C_{TPA}}{\Phi_A^2} - \left(\frac{k_1}{K_1} \right) \frac{C_W C_{tTPA}}{\Phi_A^2} \left\{ \frac{C_{tEG}}{C_{tEG} + C_{bEG}\Phi_A} \right\} \right]$
$R_2 = \Phi_A R'_2 = \Phi_A \left[2k_2 \frac{C_{EG}C_{tTPA}}{\Phi_A^2} - 2 \left(\frac{k_2}{K_2} \right) \frac{C_W C_{bTPA}}{\Phi_A^2} \left\{ \frac{C_{tEG}}{C_{tEG} + C_{bEG}\Phi_A} \right\} \right]$
$R_3 = \Phi_A R'_3 = \Phi_A \left[2k_3 \frac{C_{tEG}C_{TPA}}{\Phi_A^2} - \left(\frac{k_3}{K_3} \right) \frac{C_W C_{tTPA}}{\Phi_A^2} \left\{ \frac{C_{bEG}\Phi_A}{C_{tEG} + C_{bEG}\Phi_A} \right\} \right]$
$R_4 = \Phi_A R'_4 = \Phi_A \left[k_4 \frac{C_{tEG}C_{TPA}}{\Phi_A^2} - 2 \left(\frac{k_4}{K_4} \right) \frac{C_W C_{bTPA}}{\Phi_A} \left\{ \frac{C_{bEG}\Phi_A}{C_{tEG} + C_{bEG}\Phi_A} \right\} \right]$
$R_5 = \Phi_A R'_5 = \Phi_A \left[k_5 \frac{C_{tEG}^2}{\Phi_A^2} - 4 \left(\frac{k_5}{K_5} \right) \frac{C_{EG}C_{bEG}}{\Phi_A} \right]$
$R_6 = \Phi_A R'_6 = \Phi_A k_6 \frac{C_{tEG}^2}{\Phi_A^2}$
$R_7 = \Phi_A R'_7 = \Phi_A k_7 C_{bEG} \frac{C_{bTPA}\Phi_A}{C_{tEG} + C_{bEG}\Phi_A}$
$R_8 = \Phi_A R'_8 = \Phi_A k_8 \frac{C_{tEG}}{\Phi_A} C_{bEG} \frac{C_{bTPA}\Phi_A}{C_{tEG} + C_{bEG}\Phi_A}$
$R_9 = \Phi_A R'_9 = \Phi_A k_9 \frac{C_{tEG}C_{tVIN}}{\Phi_A^2}$

chemical reactions, and it can be expressed by a combination of the reaction rates R_i ($i = 1-9$). $G_j(t)$ and R_i are listed in Tables IV and V. The diffusion process was assumed to be Fickian and isothermal without a volume change of the particle. The relevant boundary and initial conditions for eqs. (1) and (2) are as follows:

$$C_j = C_j^S \quad \text{for } t > 0, r = r_s \quad (3)$$

$$\frac{\partial C_j}{\partial r} = 0 \quad \text{for } t > 0, r = 0 \quad (4)$$

$$C_j = C_j^0 \quad \text{for } t = 0, 0 < r < r_s \quad (5)$$

An assumption was made by Mallon and Ray⁹ and Wu and Chen¹¹ that all SSP reactions take place only in the amorphous region and that all the monomers and chain end groups exist only in the amorphous region because they are expelled from the crystalline phase. All the reaction rates should, therefore, be calculated, on the basis of the amorphous region only. The concentrations of monomers, end groups, and byproducts should be modified for the same reason, as shown in eqs. (6) and (7):

$$R'_i = \frac{R_i}{\Phi_A} \quad (6)$$

$$C'_j = \frac{C_j}{\Phi_A} \quad (7)$$

where i is 1–9; j is TPA, EG, W, AA, tEG, tTPA, or tVIN; Φ_A is the volume fraction of the amorphous region; R_i is the reaction rate based on the entire volume of a pellet; R'_i is the reaction rate based on the amorphous region; C_j is the concentration based on the entire volume of a pellet; and C'_j is the converted concentration based on the amorphous region. For repeat units (bEG, bTPA, and bDEG), C_j is the same as C'_j because those species have been assumed to exist homogeneously over both the amorphous and crystalline regions. Assumptions concerning the uniform distributions of the aforementioned repeat units have been made to simplify the model. Future modifications will address distribution variations.

Application of the Crank–Nicolson method to the SSP model

The finite difference method was used to solve differential equations in the model. There are 10 governing equations for each component in the model, as shown in eqs. (1) and (2). Three equations are partial differential equations, each of which has one dependent variable, the concentration, and two independent variables, the position (radius) in a pellet and SSP time. The remaining seven equations are ordinary differential equations. As mentioned earlier, the Crank–Nicolson method was used to solve three partial differential equations. A general form of the partial differential equations follows:

$$\frac{\partial g}{\partial t} = D_g \left(\frac{\partial^2 g}{\partial r^2} + \frac{2}{r} \frac{\partial g}{\partial r} \right) + G_g \quad (8)$$

where g ($\equiv C_{EG}$) is the concentration of EG in a PET pellet, r is the radius in a pellet assuming spherical coordinates, D_g is the diffusivity of EG in a PET pellet, and G_g is the generation term due to chemical reactions that involve EG. G_g can be expressed as a function of the concentrations of components at a certain time for different radii, according to Tables IV and V. By solving eq. (8) numerically, we can obtain g values according to times and positions, as expressed in Figure 1.

With the Crank–Nicolson method,²² the equation can be rewritten in the finite difference form as follows:

$$\begin{aligned} \frac{g_i^{l+1} - g_i^l}{\Delta t} = D_g \left[\frac{1}{2} \left(\frac{g_{i+1}^l - 2g_i^l + g_i^l}{(\Delta r)^2} \right. \right. \\ \left. \left. + \frac{g_{i+1}^{l+1} - 2g_i^{l+1} + g_i^{l+1}}{(\Delta r)^2} \right) + \frac{2}{r} \left\{ \frac{1}{2} \left(\frac{g_{i+1}^l - g_i^l}{\Delta r} \right. \right. \right. \\ \left. \left. \left. + \frac{g_{i+1}^{l+1} - g_i^{l+1}}{\Delta r} \right) \right\} \right] + G_g \quad (9) \end{aligned}$$

The subscript i denotes the index along the radius coordinate, and the superscript l denotes the index

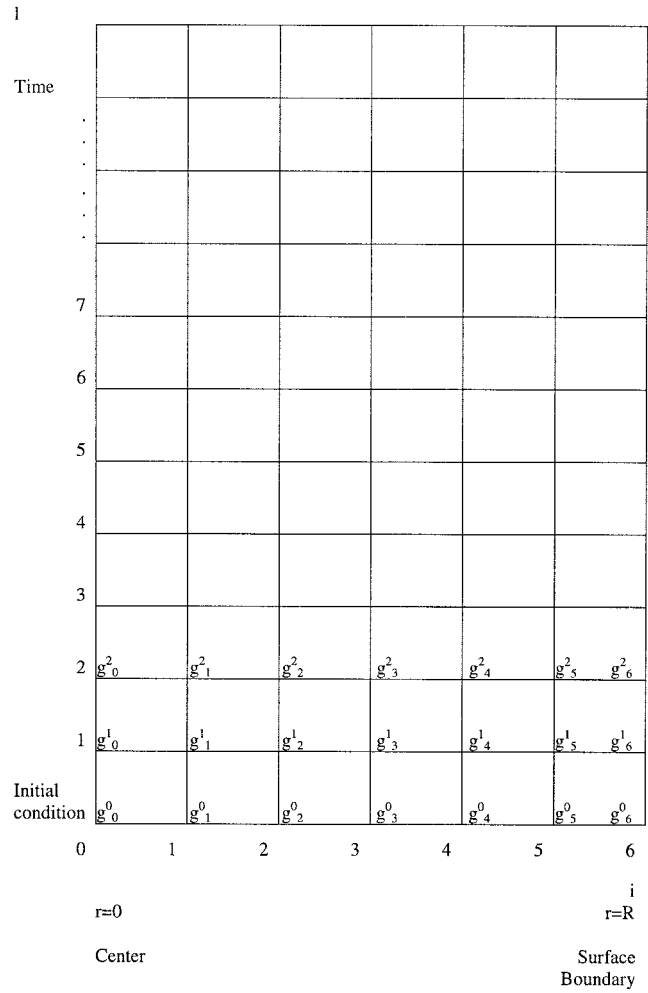


Figure 1 Radius and time coordinates of the numerical analysis for one spherical PET pellet.

along the time coordinate. Δt and Δr denote the magnitude of one grid in time and radius, respectively, where the difference equation is solved. If we rearrange the equation, we obtain

$$\begin{aligned} g_i^{l+1} - g_i^l = \lambda \{ g_{i+1}^l - 2g_i^l + g_i^l + g_{i+1}^{l+1} - 2g_i^{l+1} + g_i^{l+1} \\ + \kappa (g_{i+1}^l - g_i^l + g_{i+1}^{l+1} - g_i^{l+1}) \} + (\Delta t) G_g \quad (10) \end{aligned}$$

where λ and κ are defined by eqs. (11) and (12). κ is not a constant but a matrix containing five components along the radius axis:

$$\lambda \equiv \frac{(\Delta t) D_g}{2(\Delta r)^2} \quad (11)$$

$$\begin{aligned} \kappa \equiv \frac{2(\Delta r)}{r} = \left[\frac{2(\Delta r)}{r_1}, \frac{2(\Delta r)}{r_2}, \frac{2(\Delta r)}{r_3}, \frac{2(\Delta r)}{r_4}, \frac{2(\Delta r)}{r_5} \right] \\ = [\kappa_1, \kappa_2, \kappa_3, \kappa_4, \kappa_5] \quad (12) \end{aligned}$$

g values with subscript $l+1$ indicate the values of one step forward in the time axis, one-step future values,

that we want to solve. If we rearrange eq. (10) again after arranging all the future values into the left side,

$$-\lambda g_{i-1}^{l+1} + (1 + 2\lambda + \kappa_1 \lambda) g_i^{l+1} - \lambda(\kappa + 1) g_{i+1}^{l+1} = \lambda g_{i-1}^l + (1 - 2\lambda - \kappa \lambda) g_i^l + \lambda(\kappa + 1) g_{i+1}^l + (\Delta t) G_g \quad (13)$$

The next step is to apply this finite equation to our system, which is one PET pellet. The index i changes from 0 to 7 in the radial direction as r changes from the pellet center to the surface.

For $i = 1$, the equation becomes

$$-\lambda g_0^{l+1} + (1 + 2\lambda + \kappa_1 \lambda) g_1^{l+1} - \lambda(\kappa_1 + 1) g_2^{l+1} = \lambda g_0^l + (1 - 2\lambda - \kappa_1 \lambda) g_1^l + \lambda(\kappa_1 + 1) g_2^l + (\Delta t) G_{g,i=1} \quad (14)$$

Likewise, if we consider the cases of $i = 2-5$, we get four more finite difference equations:

$$\begin{pmatrix} 1 + \lambda + \kappa_1 \lambda & -\lambda(\kappa_1 + 1) & 0 & 0 & 0 \\ -\lambda & 1 + 2\lambda + \kappa_2 \lambda & -\lambda(\kappa_2 + 1) & 0 & 0 \\ 0 & -\lambda & 1 + 2\lambda + \kappa_3 \lambda & -\lambda(\kappa_3 + 1) & 0 \\ 0 & 0 & -\lambda & 1 + 2\lambda + \kappa_4 \lambda & -\lambda(\kappa_3 + 1) \\ 0 & 0 & 0 & -\lambda & 1 + 2\lambda + \kappa_5 \lambda \end{pmatrix} \begin{pmatrix} g_1^{l+1} \\ g_2^{l+1} \\ g_3^{l+1} \\ g_4^{l+1} \\ g_5^{l+1} \end{pmatrix} = \begin{pmatrix} \lambda g_0^l + (1 - 2\lambda - \kappa_1 \lambda) g_1^l + \lambda(\kappa_1 + 1) g_2^l + (\Delta t) G_{g,i=1} \\ \lambda g_1^l + (1 - 2\lambda - \kappa_2 \lambda) g_2^l + \lambda(\kappa_2 + 1) g_3^l + (\Delta t) G_{g,i=2} \\ \lambda g_2^l + (1 - 2\lambda - \kappa_3 \lambda) g_3^l + \lambda(\kappa_3 + 1) g_4^l + (\Delta t) G_{g,i=3} \\ \lambda g_3^l + (1 - 2\lambda - \kappa_4 \lambda) g_4^l + \lambda(\kappa_4 + 1) g_5^l + (\Delta t) G_{g,i=4} \\ \lambda g_4^l + (1 - 2\lambda - \kappa_5 \lambda) g_5^l + \lambda(\kappa_5 + 1) g_6^l + (\Delta t) G_{g,i=5} \end{pmatrix} \quad (19)$$

$$\begin{pmatrix} g_1^{l+1} \\ g_2^{l+1} \\ g_3^{l+1} \\ g_4^{l+1} \\ g_5^{l+1} \end{pmatrix} = \begin{pmatrix} 1 + \lambda + \kappa_1 \lambda & -\lambda(\kappa_1 + 1) & 0 & 0 & 0 \\ -\lambda & 1 + 2\lambda + \kappa_2 \lambda & -\lambda(\kappa_2 + 1) & 0 & 0 \\ 0 & -\lambda & 1 + 2\lambda + \kappa_3 \lambda & -\lambda(\kappa_3 + 1) & 0 \\ 0 & 0 & -\lambda & 1 + 2\lambda + \kappa_4 \lambda & -\lambda(\kappa_3 + 1) \\ 0 & 0 & 0 & -\lambda & 1 + 2\lambda + \kappa_5 \lambda \end{pmatrix}^{-1} \begin{pmatrix} \lambda g_0^l + (1 - 2\lambda - \kappa_1 \lambda) g_1^l + \lambda(\kappa_1 + 1) g_2^l + (\Delta t) G_{g,i=1} \\ \lambda g_1^l + (1 - 2\lambda - \kappa_2 \lambda) g_2^l + \lambda(\kappa_2 + 1) g_3^l + (\Delta t) G_{g,i=2} \\ \lambda g_2^l + (1 - 2\lambda - \kappa_3 \lambda) g_3^l + \lambda(\kappa_3 + 1) g_4^l + (\Delta t) G_{g,i=3} \\ \lambda g_3^l + (1 - 2\lambda - \kappa_4 \lambda) g_4^l + \lambda(\kappa_4 + 1) g_5^l + (\Delta t) G_{g,i=4} \\ \lambda g_4^l + (1 - 2\lambda - \kappa_5 \lambda) g_5^l + \lambda(\kappa_5 + 1) g_6^l + (\Delta t) G_{g,i=5} \end{pmatrix} \quad (20)$$

Finally, by solving this matrix equation, we can solve for g values of one step forward in the timescale if we know these values. As we know the initial conditions, $g_{i,0}^0$, we can solve for $g_{i,1}^1$ values. Likewise, other concentrations for other components at $l = 1$ can be obtained if the initial concentrations ($l = 0$) are known. It is necessary to solve for the concentrations for all the components at time $l = 1$ before we solve for the concentrations at time $l = 2$ because all the components are required to estimate nine reaction rates at this time. Once all the concentrations are solved at time $l = 1$, then the concentrations at time $l = 2$ can be solved in the same way. If we continue to solve for g values by moving along the time axis, l , we can solve

$$-\lambda g_1^{l+1} + (1 + 2\lambda + \kappa_2 \lambda) g_2^{l+1} - \lambda(\kappa_2 + 1) g_3^{l+1} = \lambda g_1^l + (1 - 2\lambda - \kappa_2 \lambda) g_2^l + \lambda(\kappa_2 + 1) g_3^l + (\Delta t) G_{g,i=2} \quad (15)$$

$$-\lambda g_2^{l+1} + (1 + 2\lambda + \kappa_3 \lambda) g_3^{l+1} - \lambda(\kappa_3 + 1) g_4^{l+1} = \lambda g_2^l + (1 - 2\lambda - \kappa_3 \lambda) g_3^l + \lambda(\kappa_3 + 1) g_4^l + (\Delta t) G_{g,i=3} \quad (16)$$

$$-\lambda g_3^{l+1} + (1 + 2\lambda + \kappa_4 \lambda) g_4^{l+1} - \lambda(\kappa_4 + 1) g_5^{l+1} = \lambda g_3^l + (1 - 2\lambda - \kappa_4 \lambda) g_4^l + \lambda(\kappa_4 + 1) g_5^l + (\Delta t) G_{g,i=4} \quad (17)$$

$$-\lambda g_4^{l+1} + (1 + 2\lambda + \kappa_5 \lambda) g_5^{l+1} - \lambda(\kappa_5 + 1) g_6^{l+1} = \lambda g_4^l + (1 - 2\lambda - \kappa_5 \lambda) g_5^l + \lambda(\kappa_5 + 1) g_6^l + (\Delta t) G_{g,i=5} \quad (18)$$

The previous five equations can be rewritten as a matrix-type equation. After applying boundary conditions, which are $g_0 = g_1$ and $g_6 = g_5 = 0$, we obtain one set of matrix equations:

for g values completely as a function of position and time.

Diffusivities and reaction rate constants

The free-volume theory, already used by Kang¹⁵ and Devotta and Mashelkar,¹⁶ can be used to obtain the diffusivities of the volatile components. According to the free volume theory, the diffusivity of a diffusing small molecule in a very concentrated polymer solution can be obtained as follows:

$$D_j = RTA_j e^{[-B_j/V_j]} \quad (21)$$

TABLE VI
Adjusted Kinetic Rate Constants Used in the Model as a Function of Temperature (T) in K,
and the Degree of Polymerization (X_n)

i	k_i (L/mol/min)	K_i
1	$14 \times 10^{12} \times (100/X_n)^2 \times \exp(-13,500/1.987/T) \times \exp(-17,600/1.987/T)$	2.5
2	$14 \times 10^{12} \times (100/X_n)^2 \times \exp(-13,500/1.987/T) \times \exp(-17,600/1.987/T)$	2.5
3	$7 \times 10^{12} \times (100/X_n)^2 \times \exp(-13,500/1.987/T) \times \exp(-17,600/1.987/T)$	1.25
4	$1.2 \times 10^{13} \times k_0 \times (100/X_n)^2 \times \exp(-13,500/1.987/T) \times \exp(-17,600/1.987/T)$	1.25
5	$5.4 \times 10^{12} \times k_0 \times (100/X_n)^2 \times \exp(-13,500/1.987/T) \times \exp(-18,500/1.987/T)$	0.5
6	$1.8 \times 10^{15} \times (100/X_n)^2 \times \exp(-13,500/1.987/T) \times \exp(-29,800/1.987/T)$	—
7	$8 \times 10^9 \times \exp(-37,800/1.987/T)^a$	—
8	$3 \times 10^9 \times \exp(-29,800/1.987/T)^a$	—
9	$2 \times 10^{12} \times (100/X_n)^2 \times \exp(-13,500/1.987/T) \times \exp(-18,500/1.987/T)$	—

^a The units of reactions 7 and 8 are L/min.

where j is EG, W, or AA; A_j is the prefactor; B_j is the so-called jump factor of the diffusing component; V_f is the effective fractional free volume of the system; R is the gas constant; and T is the temperature (K). B_j depends on the size and shape of the diffusing molecule. Values estimated by Kulkarni and Mashelkar²³ were used to determine B_j in this model. In eq. (21), V_f can be given by

$$V_f = f_A \Phi_A + f_{EG} \Phi_{EG} + f_W \Phi_W \quad (22)$$

where f_A , f_{EG} , and f_W denote the fractional free volumes of the amorphous phase, EG, and W, respectively, and Φ 's are the volume fractions in the system. Φ_A can be determined from the crystallinity data as long as the crystallinity is a function of temperature only (the crystallinity does not change significantly during SSP, except during an initial short period of time). The contributions from the crystalline phase, the carrier gas used, and the other volatile byproducts (EG, W, and AA) are not considered in this equation. f_A can be obtained from the equation:²⁴

$$f_A = f_g + \alpha(T - T_g) \quad (23)$$

where f_g is the fractional free volume at the glass-transition temperature (T_g) of the polymer and α is the thermal expansion coefficient of the free volume. For simplicity, the effect of the molecular weight on T_g was not considered.

Above T_g , amorphous polymer chains have translational degrees of freedom. In comparison with the corresponding melt polymerization process, the chain mobility during SSP is relatively low because of the low reaction temperature and the different state of the material. The chain mobility was determined by Kang¹⁵ from reptation theory and an Arrhenius-type relation; therefore, the reaction rate constants between the reactive polymer chains can be expressed as functions of the chain mobility and the activation energy of the reaction:

$$k_i = A_i \left(\frac{X_R}{X_n} \right)^2 e^{[-E_p/RT]} e^{[-E_i/RT]} \quad (24)$$

where i is 1–3, 6, or 9; A_i is the prefactor; X_R is the number-average degree of polymerization for a reference state (here 100); X_n is the number-average degree of polymerization at any time; E_p is the activation energy for the translational motion, which was 13.5 kcal/mol from rheological data for molten PET;^{15,25} and E_i is the activation energy of reaction i . Among these reaction rate constants, the rate constants for the main polymerization reactions (reactions 4 and 5) were modified as follows so that k_0 could be used as a parameter for fitting the simulation results to the experimental data:

$$k_i = A_i k_0 \left(\frac{X_R}{X_n} \right)^2 e^{[-E_p/RT]} e^{[-E_i/RT]} \quad (25)$$

where i is 4 or 5. Because reactions 7 and 8 are intramolecular reactions, not affected by the translational motion of polymer chains, the rate constant for them can be written as follows:

$$k_i = A_i e^{[-E_i/RT]} \quad (26)$$

where i is 7 or 8. X_n of the polymer chains produced can be defined as

$$X_n = \frac{C_{IEG} + C_{ITPA} + C_{bEG} + C_{bTPA} + C_{bDEG} + C_{iVIN}}{C_{IEG} + C_{ITPA} + C_{iVIN}} \quad (27)$$

The number-average molecular weight (M_n) can be calculated from the degree of polymerization by the multiplication of X_n by the molecular weight of a repeat unit:

$$M_n = M_{n0} \times X_n = 192X_n \quad (28)$$

An M_n value for the entire pellet at a certain time can then be calculated by integration over all the positions:

TABLE VII
Initial and Boundary Conditions for Each Component Used in the Modeling

Component (<i>j</i>)	Initial condition	Boundary condition
TPA (mol/L)	0.00004	—
EG (mol/L)	0	0
W (mol/L)	0	0
tEG (mol/L)	0.111	—
tTPA (mol/L)	0.056	—
bEG (mol/L)	7.145	—
bTPA (mol/L)	7.291	—
bDEG (mol/L)	0.146	—
tVIN (mol/L)	0.0004	—
AA (mol/L)	0.0008	0

For entries marked with a dash, no boundary data were required.

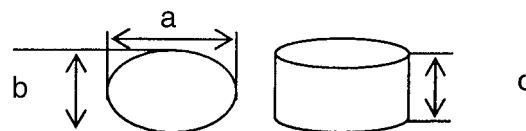
$$M_{n,avg} = \frac{\int 4\pi r^2 M_n(r) dr}{\frac{4}{3}\pi R^3} = \frac{4\pi \Delta r [\sum r^2 M_n(r)]}{\frac{4}{3}\pi R^2} \quad (29)$$

Most kinetic data, such as activation energies and frequency factors, needed for the calculation of reaction rate constants were taken from Kang's article,¹⁵ as given in Table VI. The kinetic parameters of the main reactions (k_4 and k_5), however, were adjusted with a fitting parameter (k_0). Crystallinity data were taken from our measurements.¹

The initial conditions and boundary conditions for the 10 components used are listed in Table VII. The initial concentrations of bTPA and bEG were calculated from the initial M_n of the precursor. Initial bDEG concentrations were assumed to be 2 mol % (based on the total moles of the base monomer). The initial concentrations of hydroxyl and carboxyl end groups were obtained from the results of end-group analysis. The AA contents for the initial conditions were assumed to be 25 ppm (8×10^{-4} mol/L). Vinyl ester end-group contents were determined by the measurement of the AA generation rate for the precursors to give an initial condition of 4.3×10^{-4} mol/L. A detailed method for the calculation of vinyl ester end-group contents is given in the third article of this series.²⁶ The initial conditions for the contents of the TPA monomer in the

TABLE IX
Average Dimensions of the Pellets Used

Precursor	IV (dL/g)	Pellet size (mm)			Effective radius (mm)
		a	b	c	
TPA-based	0.56	2.8	2.0	2.4	1.25



precursors were assumed to be 5 ppm (4×10^{-5} mol/L).

The crystallinities of the samples were assumed to change only according to the SSP temperature, not according to the SSP time. This assumption is acceptable because the crystallinity changes only during the initial period of SSP while temperatures stabilize, after which it remains fairly stable.¹ Diffusivity values used in the modeling are listed in Table VIII.

EXPERIMENTAL

A bench-scale SSP system was set up to perform SSP experiments, as described previously.¹ Experimental data for PET precursors of IV = 0.56 were used to evaluate the fit of the modeling results. The dimensions of the precursor are described in Table IX. The effective radius was calculated with the following relationship:⁹

$$r_{avg} = \sqrt{\frac{3}{\frac{1}{a^2} + \frac{1}{b^2} + \frac{1}{c^2}}} \quad (30)$$

After SSP experiments at various temperatures (180–230°C) and times (4, 8, and 12 h), solid-stated PET samples were taken for characterization. Melt viscosities were measured for each sample, and equivalent IV and M_n values were calculated to provide data to compare and fit with simulation results. Crystallinities

TABLE VIII
Crystallinities, Fitting Parameters, and Diffusivity Values for Volatile Components (EG, W, and AA) Used in the Model

SSP temperature (°C)	Crystallinity (vol %)	k_0^a	D_{EG} ($\times 10^{-6}$ cm ² /s)	D_W ($\times 10^{-6}$ cm ² /s)	D_{AA} ($\times 10^{-6}$ cm ² /s)
180	49	0.14	3.00	7.91	3.77
190	52	0.14	3.05	8.06	3.84
200	54	0.14	3.14	8.26	3.95
210	56	0.13	3.24	8.48	4.07
220	59	0.11	3.19	8.51	4.02
230	62	0.13	3.14	8.57	3.99

^a Fitting parameter in the rate constants for reactions 4 and 5 in Table VII.

were estimated by the measurement of the densities of samples and were used as input data. The contents of carboxyl end groups, measured with FTIR spectroscopy, were also compared with modeling results. The contents of hydroxyl end groups, obtained by the subtraction of the contents of carboxyl end groups from the total end-group contents, were obtained from calculations with M_n 's. Detailed descriptions of the SSP system, SSP experiments, and characterization techniques are included in the first article of this series.¹

RESULTS AND DISCUSSION

We performed modeling studies to simulate SSP experiments by adjusting a fitting parameter (k_0). After confirming that the molecular weight modeling results successfully fit the experimental data, we discuss various results from the modeling. The comprehensive model produces a great deal of useful information, giving not only molecular weights but also the concentrations of many components involved in the model. The model is useful as a means of observing the specific effects of changes in selected variables. The effects of the pellet size and the initial end-group concentration ratios on the SSP rates and vinyl ester contents are discussed.

Changes in the molecular weight and various components during SSP

Figures 2–4 show simulation results projecting molecular weight increases obtained during SSP at temperatures of 180, 200, and 230°C, respectively, as functions of times and positions in a PET pellet. When the SSP

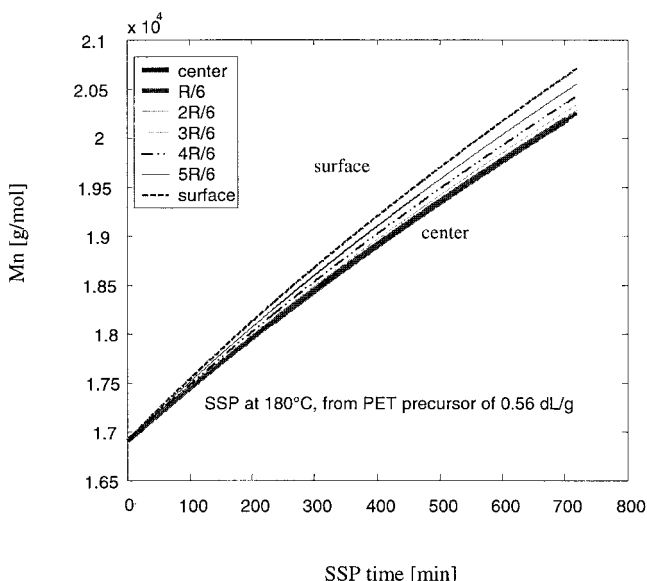


Figure 2 Simulation results projecting the M_n increase during SSP at 180°C.

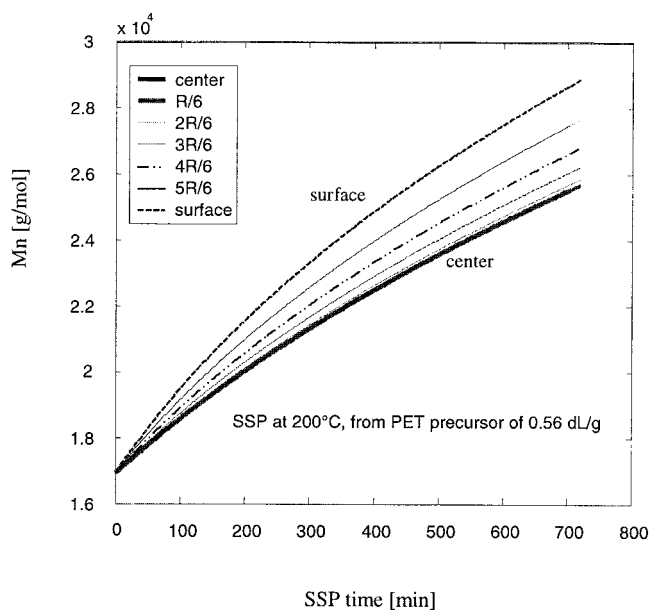


Figure 3 Simulation results projecting the M_n increase during SSP at 200°C.

temperature is low, M_n increases linearly with time, and the differences according to position in a pellet are negligible. As the SSP temperatures increase, M_n increases nonlinearly, and the differences in M_n according to positions in a pellet increase. A higher SSP rate is obtained at the surface of a pellet than at the center because the surface location is superior in terms of the diffusion of byproducts from the pellet. The M_n values were averaged for all the positions in a pellet under the assumption of a spherical pellet shape with eq. (29). These average values are compared in Figure 5 to

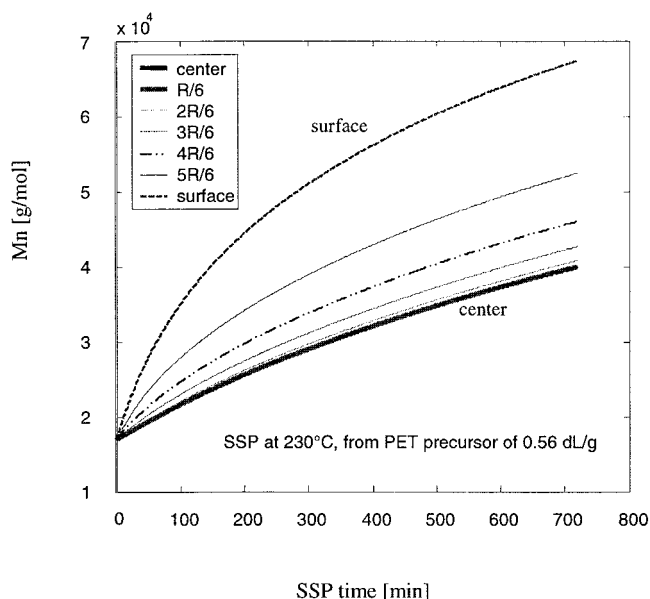


Figure 4 Simulation results projecting the M_n increase during SSP at 230°C.

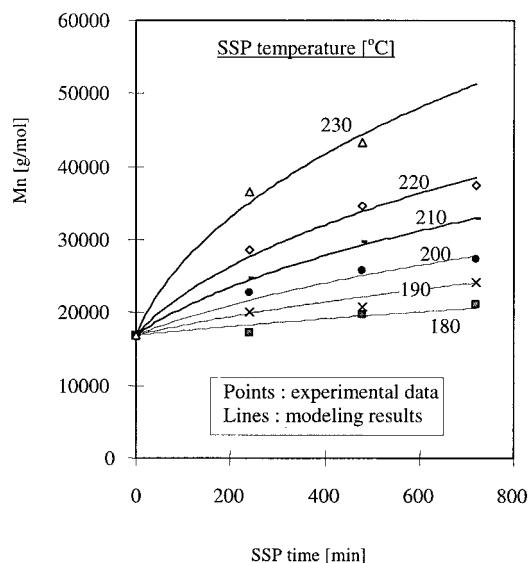


Figure 5 Result of fitting the simulation results of M_n increases in comparison with the experimental data.

the experimental data we obtained earlier.¹ All the simulation results can be fitted successfully to the experimental data with one fitting parameter (k_0), and this shows that the model predicts the experimental data very well.

The concentrations of the hydroxyl and carboxyl end groups decrease as SSP proceeds. Comparisons with the experimental data, shown in Figures 6 and 7, indicate that the simulation results follow the same trends as the experimental data, despite some differences in values. This indicates that the kinetic parameters used in the modeling are acceptable. This model does not treat the reactivity of the end groups as

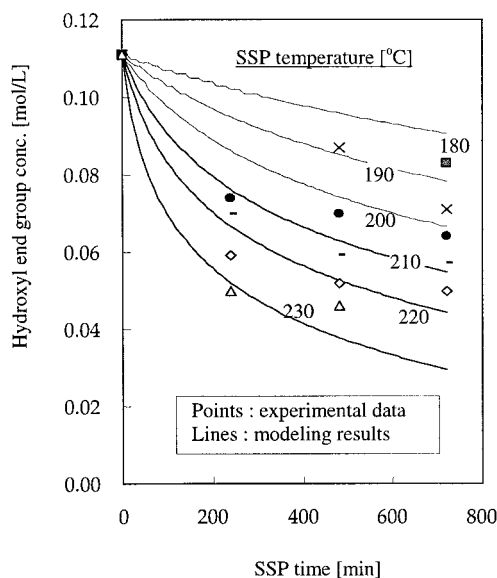


Figure 6 Modeling results for the concentration of hydroxyl end groups during SSP.

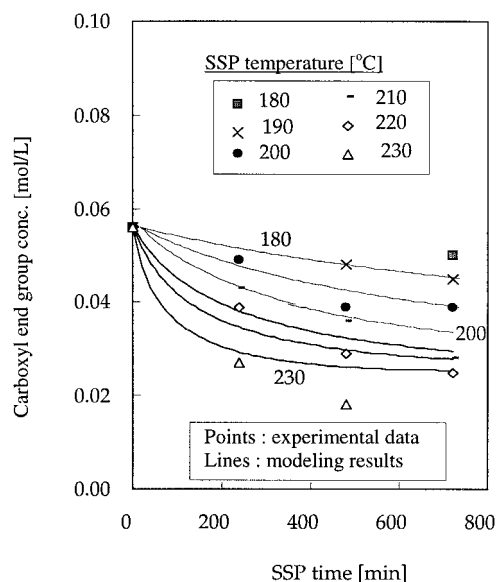


Figure 7 Modeling results for the concentration of carboxyl end groups during SSP.

rigorously as might be desired because initial efforts have been directed toward fitting changes in the molecular weight rather than the end-group concentrations. Future modifications of the model will attempt to overcome this weakness and reduce deviations from experimental results.

PET precursors generally contain some AA because of the thermal degradation that is unavoidable in melt-phase polymerization. As shown in Figure 8, the AA contents were calculated with the model to decrease as a result of diffusion during the SSP process.

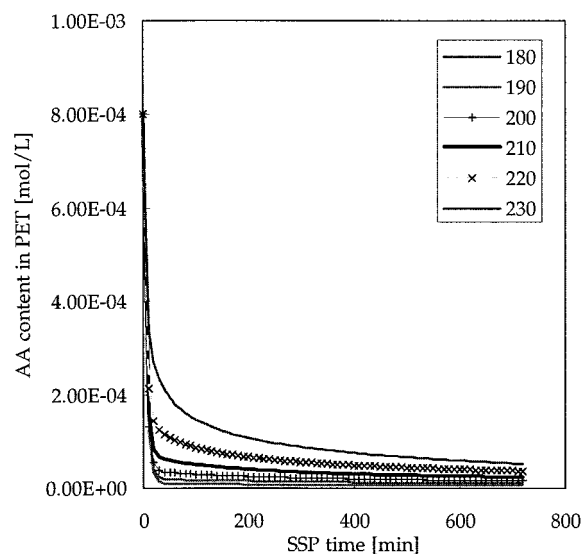


Figure 8 Modeling results for the concentration of AA in a PET pellet during SSP. The numbers in the legend denote the temperatures ($^{\circ}\text{C}$).

This decrease in AA is desirable from a material point of view for food packaging applications.

Changes in the concentrations of vinyl end groups were also simulated with the model, as shown in Figure 9. The vinyl ester end group is known as an intermediate material in one degradation reaction path to AA.¹⁹ Despite the small concentrations compared with those of other major end groups, vinyl end groups can be considered important from the aspect of thermal stability in terms of AA generation.^{3,19} The concentrations of vinyl ester end groups were projected to decrease during SSP. The results of the vinyl end group decreasing as a result of SSP agree well with the conventional observation that thermal stability is increased by SSP and so solid-stated materials will generate less AA than equivalent precursors. Wu et al.¹¹ reported, in contrary simulation results, that the concentration of vinyl ester groups would increase as a result of SSP. This contradictory projection might have been caused by their use of an inappropriate initial condition for the concentration of vinyl end groups, because in their modeling, the initial concentration of vinyl end groups was assumed to be zero. If the initial concentration of vinyl ester end group had been assumed to be zero, his model might have counted the amount of only the vinyl ester formation reaction (reaction 7 in Table III) without appropriately considering the rate of the vinyl ester consumption reaction (reaction 9 in Table III). In fact, precursors are thought to contain some amount of vinyl ester end groups due to degradation reactions in the melt-phase polymerization.

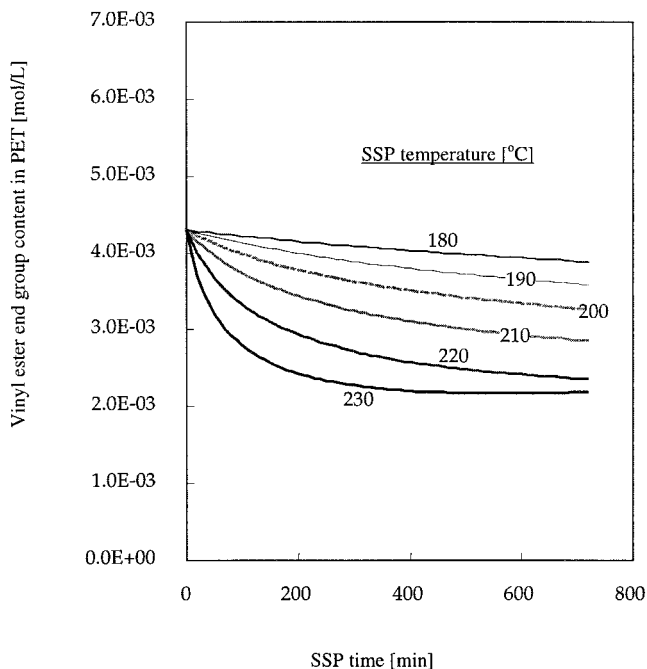


Figure 9 Modeling results for the concentration of vinyl ester end groups in a PET pellet during SSP. The numbers on the curves denote the temperatures ($^{\circ}\text{C}$).

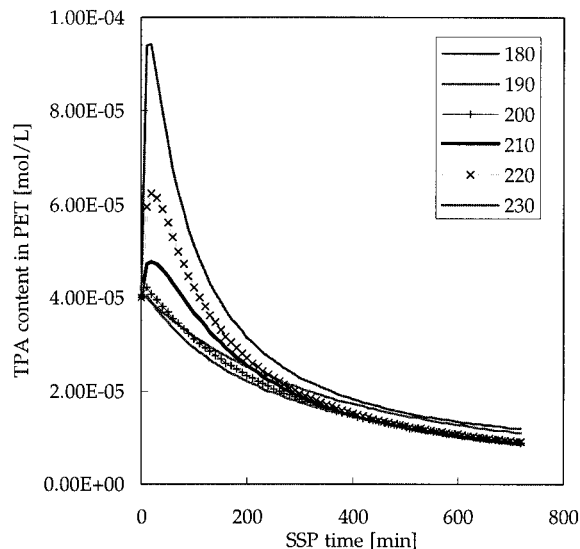


Figure 10 Modeling results for the concentration of the TPA monomer in a PET pellet during SSP. The numbers in the legend denote the temperatures ($^{\circ}\text{C}$).

TPA is one of the raw material monomers used to polymerize PET. Even though the TPA concentration is very low after polymerization, it can nevertheless cause some problems in the PET processing step because it sometimes appears as a white powder during the molding process of PET.²¹ This occurs because TPA sublimes at temperatures near 300°C .^{20,21} To avoid or minimize this problem, we must keep the concentration of TPA as low as possible. Many factors can be responsible for the presence of high concentrations of TPA. A low solubility of TPA in monomer slurries before melt-phase polymerization can be one of the causes, lowering the conversion from TPA to bis(β -hydroxy ethyl) terephthalate in the esterification step.²⁰ This, however, would be beyond the scope of this study. Other considerations can be made in terms of the reaction kinetics concerning the reversibility of polymerization reactions. If the polymerization reaction can proceed more favorably in the forward direction, it would be advantageous to keep TPA concentrations low. Simulation results indicate that the concentrations of the TPA monomer decrease during SSP, as shown in Figure 10. This can be related to the effect of a low SSP temperatures on the equilibrium of the reversible reactions because in the case of exothermic reactions, lowering the temperatures drives these reactions in a forward direction. This also indicates that the SSP process, by continuously removing reaction byproducts, is very efficient in minimizing reverse reaction rates, and this might prevail in the melt-phase polymerization. If the TPA concentration in the PET precursor is 4×10^{-5} mol/L (ca. 5 ppm), the concentration of TPA, after 12 h of SSP, can be calculated to range from 1.2×10^{-5} to 8.6×10^{-6} mol/L (1.1–1.5 ppm) according to the SSP temperatures. In terms of the reaction temperatures, conditions around 210°C

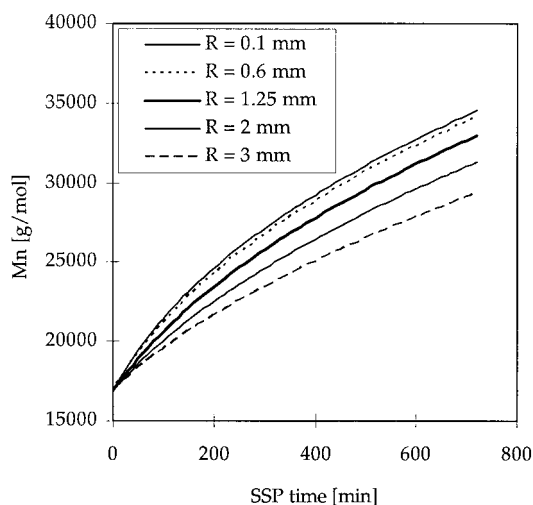


Figure 11 Modeling results for the effect of the pellet size (the radius of the pellet sphere R) on the SSP rate at 210°C.

give a minimum TPA value of 8.6×10^{-6} mol/L (ca. 1.1 ppm) in PET after SSP. It is clear that SSP helps to reduce TPA contents, but the significance of these differences in TPA concentrations is not yet clear in relationship to the SSP temperatures.

Effect of the pellet size

The effect of the pellet size on the molecular weight was simulated with the model, as shown in Figure 11. The SSP rate was projected to increase as the pellet size decreased. The effective radius of the pellets used in the experiments was around 1.25 mm. The increase in the SSP rate with decreasing pellet size can be explained by the decreases of the distance through which byproducts must diffuse to the pellet surface. The magnitude of the size effect on the SSP rate decreases as the pellet size decreases. The increase in the SSP rate due to the radius change from 0.6 to 0.1 mm is, therefore, negligible compared to that obtained when the radius is reduced from 3 to 2 mm. These results indicate that an effective radius of around 1 mm would be optimum for pellets in terms of byproduct diffusion and ease of handling.

Effect of the initial molar ratio of the end groups ([COOH]/[OH])

The initial ratio of carboxyl end groups to hydroxyl end groups was observed to affect the kinetic rates of SSP. This phenomenon is based on the differences in the rates of diffusion of EG and W from solid PET pellets. When the precursor has a very low concentration of carboxyl end groups, we cannot expect the same contribution from the esterification reaction as we would expect with higher concentrations of carboxyl end groups. This is because the esterification reaction proceeds between a carboxyl end group and a

hydroxyl end group, whereas the ester-interchange reaction occurs between two hydroxyl end groups.

Using the model, we can predict the manner in which SSP rates change according to the initial $[-\text{COOH}]/[-\text{OH}]$ molar ratio of end groups. Figure 12 shows projected molecular weight values, obtained as a function of the initial $[-\text{COOH}]/[-\text{OH}]$ molar ratio, after 12 h at SSP temperatures of 190 and 210°C. A maximum rate is obtained at a $[\text{COOH}]/[\text{OH}]$ ratio of about 0.7. This result can be compared to previous results reported by Wu et al.,¹¹ who predicted an optimum SSP rate when the $[\text{COOH}]/[\text{OH}]$ ratio was 0.5–0.8 according to SSP temperatures.

The reason that SSP rates show maximal values according to the initial molar ratio, $[\text{COOH}]/[\text{OH}]$, can be discerned from the reaction kinetics. As mentioned earlier, polymerization in SSP proceeds by two main reactions, the ester-interchange reaction and the esterification reaction. Because the overall SSP rate is determined by the sum of these two reaction rates, the changes in the rate of each reaction explain why the SSP rate shows a maximum value as the $[\text{COOH}]/[\text{OH}]$ ratio changes. The rate of the ester-interchange reaction decreases as the initial $[\text{COOH}]/[\text{OH}]$ ratio of the precursor increases, as shown in Figure 13. This is because the increase in the concentration of carboxyl end groups reduces the concentrations of hydroxyl end groups and the ester-interchange reaction rates. As shown in Figure 14, however, the rate of the esterification reaction increases as the initial $[\text{COOH}]/[\text{OH}]$ molar ratio increases up to some point, showing a maximum, and then decreases slightly at higher $[\text{COOH}]/[\text{OH}]$ ratios. Because PET generally has a $[-\text{COOH}]/[-\text{OH}]$ ratio of less than 0.6, it seems reasonable to say that the rate of esterification in-

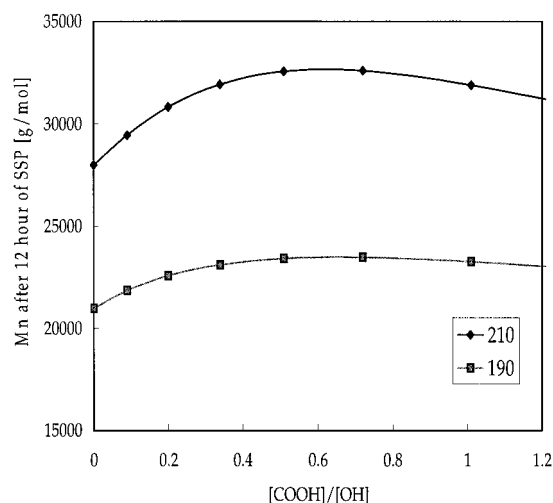


Figure 12 Effect of the initial $[-\text{COOH}]/[-\text{OH}]$ molar ratio on the SSP rate for two different SSP temperatures. The numbers in the legend denote the SSP temperatures (°C).

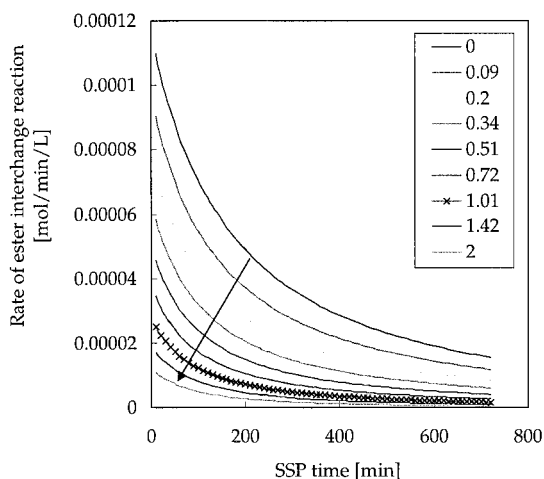


Figure 13 Effect of the initial end-group ratio on the rate of the ester-interchange reaction. The arrow shows the direction of change as $[-\text{COOH}]/[-\text{OH}]$ increases. The numbers in the legend denote the $[-\text{COOH}]/[-\text{OH}]$ ratios.

creases as the initial $[\text{COOH}]/[\text{OH}]$ molar ratio increases.

Figure 15 shows the relationships of initial end-group ratios to vinyl ester contents after SSP. The vinyl ester contents are projected to continually increase with an increasing $[\text{COOH}]/[\text{OH}]$ molar ratio. Figures 16 and 17 help to explain the reason for this result. Vinyl ester contents can be determined by the magnitudes of the vinyl ester formation reaction (reaction 7 in Table III) and the vinyl ester consumption reaction (reaction 9 in Table III). The rates of the vinyl ester formation reaction (Fig. 16) are negligible compared to those of the vinyl consumption reaction (Fig. 17), and their differences, caused by different molar ratios, are also negligible. We can now see that the

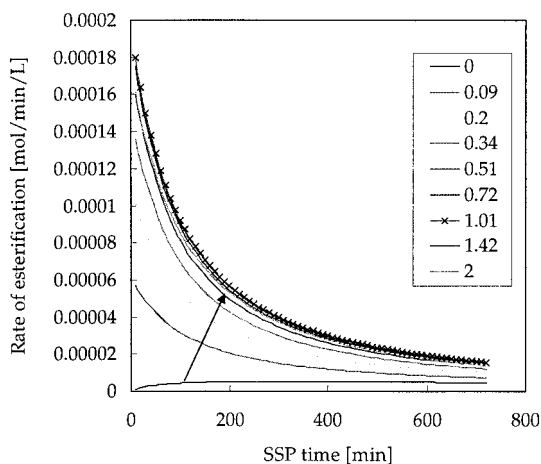


Figure 14 Effect of the initial end-group ratio on the rate of the esterification reaction. The arrow shows the direction of change as $[-\text{COOH}]/[-\text{OH}]$ increases. The numbers in the legend denote the $[-\text{COOH}]/[-\text{OH}]$ ratios.

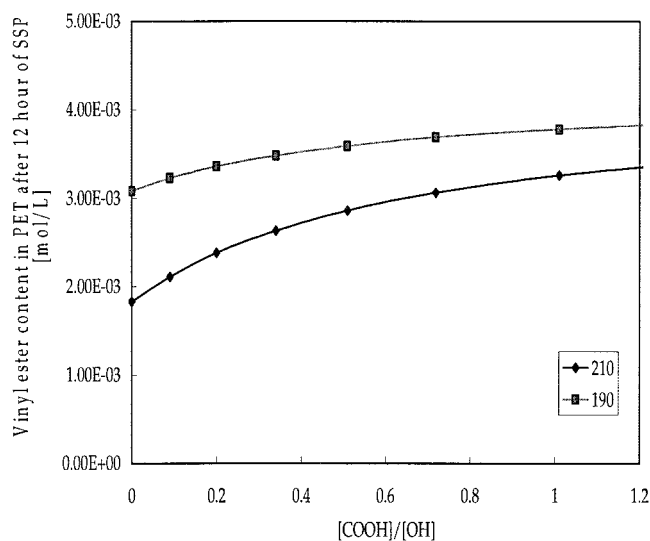


Figure 15 Simulation results for the effect of the initial $[-\text{COOH}]/[-\text{OH}]$ molar ratio on the vinyl ester contents after 12 h of SSP at two different temperatures. The numbers in the legend denote the SSP temperatures ($^{\circ}\text{C}$).

increase in the vinyl ester contents, with increasing initial $[-\text{COOH}]/[-\text{OH}]$ ratios, are caused by decreases in the vinyl ester consumption reactions.

Figure 18 shows the modeling results of the effect of the initial $[-\text{COOH}]/[-\text{OH}]$ end-group ratios on the TPA monomer contents in PET after 12 h of SSP at 190 and 210°C . As the $[-\text{COOH}]/[-\text{OH}]$ ratio increases, TPA monomer contents are projected to increase. The TPA monomer can be considered to be formed as a result of a reversed esterification reaction. If PET has lower levels of carboxyl end groups, polymerization reactions proceed more by ester-interchange reactions

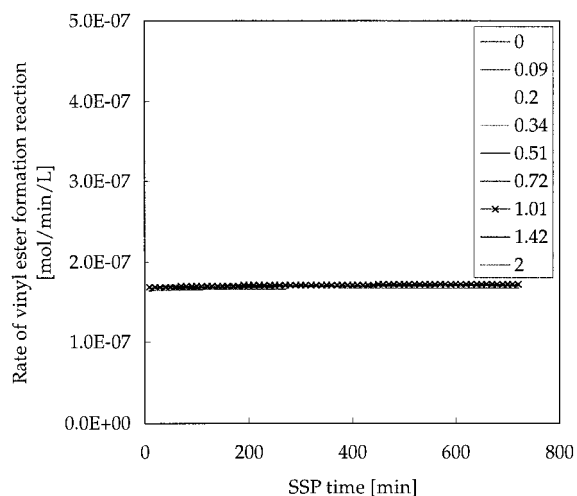


Figure 16 Effect of the initial end-group ratio on the rate of the vinyl ester formation reaction. The arrow shows the direction of change as $[-\text{COOH}]/[-\text{OH}]$ increases. The numbers in the legend denote the $[-\text{COOH}]/[-\text{OH}]$ ratio.

and less by esterification reactions and, therefore, would be less likely to form the TPA monomer.

CONCLUSIONS

The SSP model can be successfully applied to experimental data with respect to changes in M_n with one fitting parameter. The model considers 10 components, which make it possible to predict the concentrations of hydroxyl end groups, carboxyl end groups, vinyl ester end groups, and TPA monomer. This comprehensive model can be used as an efficient way of predicting changes in the contents of the vinyl ester end groups and TPA monomer, suggesting that the SSP process helps to decrease their concentrations. This is believed to be also closely related to the reduction of AA generation and TPA sublimation during the molding process.

The initial molar compositions of carboxyl end groups to hydroxyl end groups are projected by simulation to influence various SSP characteristics, including not only the SSP rate but also the concentrations of vinyl ester end groups and TPA monomer. Maximum SSP rates are obtained with an initial $[-COOH]/[-OH]$ ratio of about 0.7. As the ratio increases, the concentrations of vinyl end groups and TPA monomer also increase.

The authors thank the members of the PET Industrial Consortium who supported our research at the Polymer Institute of the University of Toledo.

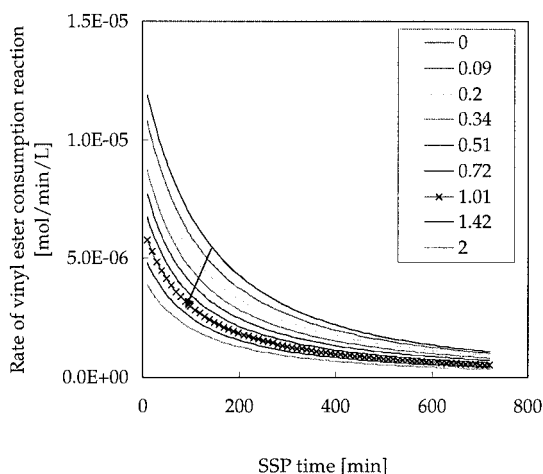


Figure 17 Effect of the initial end-group ratio on the rate of the vinyl ester consumption reaction. The arrow shows the direction of change as $[-COOH]/[-OH]$ increases. The numbers in the legend denote the $[-COOH]/[-OH]$ ratio.

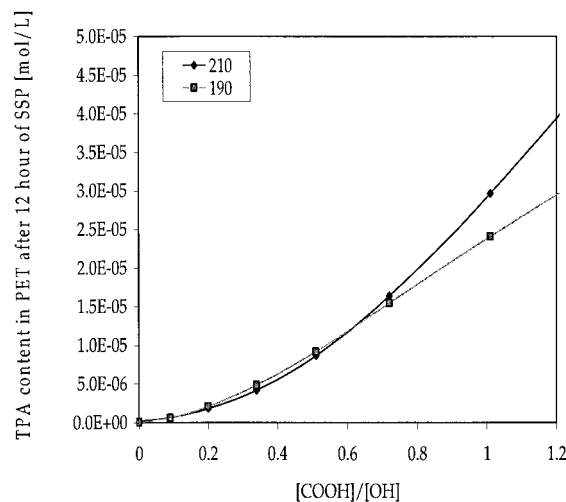


Figure 18 Simulation results for the effect of the initial $[-COOH]/[-OH]$ molar ratio on the TPA monomer contents in PET after 12 h of SSP at two different temperatures. The numbers in the legend denote the SSP temperatures ($^{\circ}C$). The initial content of the TPA monomer before SSP was assumed to be 0.00004 mol/L, or 5 ppm.

References

- Kim, T.; Lofgren, E.; Jabarin, S. *J Appl Polym Sci* 2003, 89, 197.
- Jabarin, S. In *Polymeric Materials Encyclopedia*; Salamone, J. C., Ed.; CRC: New York, 1996; Chapter 8, p 6078.
- Ravindranath, K.; Mashelkar, R. *Chem Eng Sci* 1986, 41, 2197.
- Huang, B.; Walsh, J. *Polymer* 1998, 39, 6991.
- Gao, Q.; Huang, N.; Gerking, L. *Chem Eng Sci* 1997, 52, 371.
- Ravindranath, K.; Mashelkar, R. *J Appl Polym Sci* 1990, 39, 1325.
- Chen, F.; Griskey, R.; Beyer, G. *AIChE* 1969, 15, 680.
- Chang, T. *Polym Eng Sci* 1970, 10, 364.
- Mallon, F.; Ray, W. *J Appl Polym Sci* 1998, 69, 1233.
- Chen, S.; Chen, F. *J Polym Sci Part A: Polym Chem* 1987, 25, 533.
- Wu, D.; Chen, F.; Li, R. *Macromolecules* 1997, 30, 6737.
- Jabarin, S.; Lofgren, E. *J Appl Polym Sci* 1986, 32, 5315.
- Droscher, M.; Wegner, G. *Polymer* 1978, 19, 43.
- Karayanindis, G.; Sideridou, I.; Zamboulis, D.; Stalidis, G.; Bikiaris, D.; Lazaridis, N.; Wilmes, A. *Angew Makromol Chem* 1991, 192, 155.
- Kang, C. *J Appl Polym Sci* 1998, 68, 837.
- Devotta, I.; Mashelkar, R. *Chem Eng Sci* 1993, 10, 1859.
- Yoon, K.; Kwon, M.; Jeon, M.; Park, O. *Polym J* 1993, 25, 219.
- Duh, B. *J Appl Polym Sci* 2001, 81, 1748.
- Halek, G. *J Polym Sci Polym Symp* 1986, 74, 83.
- Yuki, K. *Saturated Polyester Resin Handbook*; Nikkan Kougyo-sha: Tokyo, 1989; Chapter 2.
- Besnoin, J.; Choi, K. *J Macromol Sci Rev Macromol Chem Phys* 1989, 29, 55.
- Chapra, S.; Canale, R. *Numerical Methods for Engineers*; McGraw-Hill: New York, 1998; Chapters 25 and 30.
- Kulkarni, M.; Mashelkar, R. *Chem Eng Sci* 1983, 38, 925.
- Williams, M.; Landel, R.; Ferry, J. *J Am Chem Soc* 1955, 77, 3701.
- Gregory, D. *J Appl Polym Sci* 1972, 16, 1479.
- Kim, T.; Jabarin, S. *J Appl Polym Sci* 2003, 89, 228.